Tissue Classification Based on 3D Local Intensity Structure for Volume Rendering

Yoshinobu Sato†   Carl-Fredrik Westin†   Abhir Bhalerao†   Shin Nakajima†
Nobuyuki Shiraga†   Shigeyuki Yoshida‡   Gary Zientara†   Ron Kikinis†

† Department of Radiology, Harvard Medical School and Brigham and Women's Hospital
75 Francis St, Boston, MA 02115, USA.
‡ Dept of Radiology, Osaka University Medical School

Abstract   *This paper describes 3D image filters for the enhancement of specific local intensity structures such as line and sheet, and its application to tissue classification for volume rendering. Multi-channel classification is performed by combining different 3D image filter outputs. The resulted method significantly enlarges the scope of volume rendering, especially in the medical domain. We show the usefulness of the method for different visualization problems.*

1 Introduction

Volume rendering is a powerful visualization tool especially for medical application [1],[2],[3],[4]. Basic requirement in medical application is to visualize specific tissues of interest with the relation to surrounding structures. Tissue classification is one of the most important processes in the volume rendering pipeline. Most commonly, this process is done based on the histogram of intensity values in original 3D images. Probabilistic or fuzzy classification has been used instead of binary classification in order to relate the probability of existence of each tissue to assigned opacity and color [5]. Nevertheless, it should be noticed that the performance of a classification method is largely limited by the quality of the feature measurements however mathematically elaborate it is. In the image processing field, intensive studies have been done on obtaining and using the good feature measurements for more reliable extraction and segmentation of regions of interest. One of such efforts is the use of multi-spectral information. In the medical field, multi-spectral MR images, for example, the combination of T1-weighted and T2-weighted images, have been used for multi-channel classifiers [6],[7]. Another effort is to design and use a special-purpose image filter for the enhancement of specific tissues of interest [8]. Successful results have been shown for the extraction of curvilinear structures such as blood vessels and the bronchial tree, and blob-like shape such as tumors.

In this paper, we propose a novel approach to tissue classification in the volume rendering pipeline. The basic idea is to characterize each tissue based on not only its MR or CT values but also its local shape [9],[10]. For example, blood vessels and cortices are characterized by line-like structures and sheet-like structures, respectively. We design 3D image filters to enhance specific 3D local intensity structures and use their outputs as multi-channel information for tissue classification. The classification process can be viewed as assinging shading parameters including opacity and color to each voxel. The shading parameters are assigned using the multi-dimensional feature space whose axes correspond to the filtered values as well as original intensity values. Through the visualization using different imaging modalities and anatomical structures, we show that the 3D local intensity structures can play an important role for characterizing tissues and the resulted volume rendering images are quite useful in comprehensive visualization for interventional therapy planning and accurate diagnosis.

2 3D Local Intensity Structure

2.1 Formulation of Edge, Line, Sheet, and Blob Filters

The first and second order structures of local intensity variations around each point of a 3D image can be described by the gradient vector and the Hessian matrix, respectively. The gradient vector is defined as

$$\nabla I = (I_x, I_y, I_z) \tag{1}$$

where partial derivatives of image $I(x, y, z)$ are represented as I_x, I_y, and I_z. The gradient magnitude is given by

$$|\nabla I| = \sqrt{I_x^2 + I_y^2 + I_z^2}. \tag{2}$$

The gradient magnitude has been widely used as a measure of similarity to a 3D edge structure.

The Hessian matrix is given by

$$H = \begin{bmatrix} I_{xx} & I_{xy} & I_{xz} \\ I_{yx} & I_{yy} & I_{yz} \\ I_{zx} & I_{zy} & I_{zz} \end{bmatrix} \tag{3}$$

where partial second derivatives of image $I(x, y, z)$ are represented like I_{xx}, I_{yz}, and so on. Let the eigenvalues of H be λ_1, λ_2, λ_3 ($\lambda_1 > \lambda_2 > \lambda_3$), and their corresponding eigenvectors be $\mathbf{e}_1$, $\mathbf{e}_2$, $\mathbf{e}_3$, respectively. Three types of local structures, that is, sheet, line, and blob structures, can be classified using these eigenvalues, and the basic conditions are summarized in Table 1. The examples of anatomical structures having these local structures are also shown there. Table 1 shows the conditions in the case of bright structures as contrasted with surrounding regions. Similarly, the conditions can be specified in case that the contrast is reverse.

Table 1: Basic conditions for each local structure and examples of anatomical structures

Structure	Eigenvalue Conditions	Examples
Sheet	$\lambda_1 \simeq \lambda_2 \simeq 0, \quad 0 \gg \lambda_3.$	skin, cortex
Line	$\lambda_1 \simeq 0, \quad 0 \gg \lambda_2 > \lambda_3.$	vessel, bronchus
Blob	$0 \gg \lambda_1 > \lambda_2 > \lambda_3.$	nodule

Based on the conditions shown in Table 1, measures of similarity to these local structures can be derived. As concerns a line case, we have already proposed a similarity measure [8] given by

$$L = f_\ell(\lambda_1; \lambda_{23}) \times \lambda_{23}, \tag{4}$$

where $\lambda_{23} = \min(-\lambda_2, -\lambda_3) = -\lambda_2$, and $f_\ell(\lambda_1; \lambda_{23})$ is a function decreasing with the deviation from zero of λ_1, which is given by

$$f_\ell(\lambda_1; \lambda_{23}) = \begin{cases} \exp(-\frac{\lambda_1^2}{2(\alpha_1 \lambda_{23})^2}) & \lambda_1 \le 0, \lambda_{23} \neq 0 \\ \exp(-\frac{\lambda_1^2}{2(\alpha_2 \lambda_{23})^2}) & \lambda_1 > 0, \lambda_{23} \neq 0 \\ 0 & \lambda_{23} = 0 \end{cases} \tag{5}$$

where $\alpha_1 < \alpha_2$ (we used $\alpha_1 = 0.5$ and $\alpha_2 = 2.0$ in our experiments). $\lambda_{23} = \min(-\lambda_2, -\lambda_3) = -\lambda_2$ was based on the condition $0 \gg \lambda_2 > \lambda_3$. $f(\lambda_1; \lambda_{23})$ was multiplied in order to take into account the condition $\lambda_1 \simeq 0$. We let $f(\lambda_1; \lambda_{23})$ depend on λ_{23} for the normalization. The asymmetric characteristic of $f_\ell(\lambda_1; \lambda_{23})$ was based on the following observations:

- When λ_1 is negative, the more local structure should be regarded as blob-like shape the larger $-\lambda_1$ becomes.

- When λ_1 is positive, local structure should be regarded as stenosis-like shape which occurs due to signal loss such as partial volume effect as well as its original shape.

Therefore, when λ_1 is positive, we make the decrease with the deviation from zero of λ_1 less steep in order to recover the original shape from corrupted one as well as preserve stenosis-like shape [8].

The measure of similarity to a line structure can be extended to the blob and sheet cases. In the blob case, based on the condition $0 \gg \lambda_1 > \lambda_2 > \lambda_3$, we can use a similarity measure given by

$$B = \lambda_{123}, \tag{6}$$

where $\lambda_{123} = \min(-\lambda_1, -\lambda_2, -\lambda_3) = -\lambda_1$, which is a natural extension of λ_{23} in Eq.(6).

In the sheet case, we use a similarity measure given by

$$S = f_s(\lambda_1, \lambda_2; \lambda_3) \times (-\lambda_3), \tag{7}$$

$f_s(\lambda_1, \lambda_2; \lambda_3)$ is a function decreasing with the deviation from zero of λ_1 and λ_2, which is given by

$$f_s(\lambda_1, \lambda_2; \lambda_3) = \min(f_\ell(\lambda_1; \lambda_3), f_\ell(\lambda_2; \lambda_3)). \tag{8}$$

We used $\alpha_1 = 0.5$ and $\alpha_2 = 2.0$ in $f_\ell(\lambda_1; \lambda_3)$ and $f_\ell(\lambda_2; \lambda_3)$ in the same way as Eq.(5). The conditions $\lambda_1 \simeq 0$ and $\lambda_2 \simeq 0$ is realized by combining $f_\ell(\lambda_1; \lambda_3)$ and $f_\ell(\lambda_2; \lambda_3)$ using the min operation.

2.2 Multi-Scale Computation and Integration of Local Structures

The derivative computation of the gradient vector and the Hessian matrix is combined with Gaussian convolution. The local structures may exist at various scales. For example, bronchial trees and cortices of bone can be regarded as line structures and sheet structures with different widths, respectively. The standard deviation of Gaussian convolution can be adjusted so that the maximum filter response is given at the specific width. Multi-scale integration of the filter responses has been shown to be useful for the enhancement of various widths of curvilinear structures in 3D and 2D images and blob structures in 2D images [11],[12],[8]. A typical integration method is to normalize filter outputs of each scale and select the maximum response among multiple scales. The method can be naturally extended for other local structures in 3D images. The normalized responses can be obtained by computing the Gaussian first and second derivatives multiplying σ and σ^2, respectively, for example, as given by

$$I_x = (\sigma \times \frac{\partial}{\partial x} G(x, y, z; \sigma)) * I(x, y, z) \tag{9}$$

and

$$I_{xx} = (\sigma^2 \times \frac{\partial^2}{\partial x^2} G(x, y, z; \sigma)) * I(x, y, z) \tag{10}$$

where $*$ represents convolution, and $G(x, y, z; \sigma)$ is an isotropic Gaussian function with standard deviation σ. In small scales, however, filter responses are often high for both local structures of interest and noise components. In order

to balance the effective enhancement of thin local structures and noise suppression, we use the following method for multi-scale integration [8]:

$$\max_i \frac{1}{n_i} L_i(x,y,z) \qquad (11)$$

where n_i is the standard deviation of noise amplitudes at scale i, and L_i is the filter response at scale i (Eq.(4) in the case of line). n_i can be estimated using the region which includes typical structures needed to be removed and does not include local structures of interest. Using this method, the estimated noise level of each scale can be equalized, and the scales giving noise-dominant responses are adaptively suppressed [8].

3 Tissue Classification Based on Local Structure

Multi-dimensional feature space can be defined whose axes represent the intensity values of an original image and the similarity measures to different local structures. The opacity function $\alpha(\mathbf{x})$ and color functions $R(\mathbf{x})$ $G(\mathbf{x})$, and $B(\mathbf{x})$ are given as a funtion of multi-dimensional variable $\mathbf{x}$. Here, $\mathbf{x}$ is a feature vector consisting of multi-channel values at each voxel. Also, multi-dimensional histograms can be plotted in this space. Given tissue class $c_i(i = 1, 2, ..n)$, the problem is to determine tissue weight $w_i(\mathbf{x})$, and select tissue color $M_i = (r_i, g_i, b_i)$ and maximum tissue opacity α_i. The opacity function $\alpha(\mathbf{x})$ and color functions $R(\mathbf{x})$ $G(\mathbf{x})$, and $B(\mathbf{x})$ can be computed using the combination of $w_i(\mathbf{x})$, M_i, and α_i.

3.1 Designing Classification Strategy

The design of the classification strategy consists of the following steps.

1. Define tissue classes $c_i(i = 1, 2, ..n)$.

2. Find the local structures to characterize each tissue class, and determine the filter types and widths to define the axes of the multi-dimensional feature space.

3. Parameterize the function shape of each tissue weight $w_i(\mathbf{x})$.

4. Determine the parameters of tissue weight $w_i(\mathbf{x})$.

Each step depends on a specific application. The first step is the process of problem definition based on the requirements of users such as clinicians and medical researchers. The second and third steps are the analysis of the problem and the design of the multi-channel classifier, respectively, by the designers. The forth step is the interactive process of parameter adjustment by the users. Typical examples of the classification strategy design are shown in the following.

3.1.1 Example 1: Classification of vessel and skin in MR images of brain

The problem is to classify each voxel into one of tissue classes c_1 = "vessel", c_2 = "skin", and c_3 = "others", given MR images (SPGR) of the brain. The aim is the visualization of vessels with surrounding structures because understanding the vessel structures is important not only as for avoiding the damage to vessels but also as landmarks in neurosurgical planning and navigation [13],[14]. The vessels and the skin have higher MR values than other tissues and they have similar values in SPGR images when the contrast medium is injected to enhance the tumor. The original MR values can be used for the classification of the "vessels and skin", and other tissues. The similarity measure to line structures can be used for the classification of the vessels and the skin because the vessels are characterized by line-like structures. The multi-scale integration method described in 2.2 is combined in order to enhance various widths of vessels. The two dimensional feature space is defined whose axes x_1 and x_2 represent the original MR value and the multi-scale line-filtered value, respectively. One of the simplest shapes of the tissue weight function $w_i(x_1, x_2)$ in two-dimensional space is a rectangular function as follows:

$$w_i(x_1, x_2) = \begin{cases} 1 & \text{if} \quad a_{i1} \leq x_1 \leq a_{i2} \quad \text{and} \quad b_{i1} \leq x_2 \leq b_{i2} \\ 0 & \text{else} \end{cases}$$
$$(12)$$

where $i = 1, 2$. a_{i1}, a_{i2}, b_{i1}, and b_{i2} are finally adjusted to obtain the optimal classification.

3.1.2 Example 2: Classification of skin and brain in MR images of baby's brain

The problem is to classify each voxel into tissue classes c_1 = "skin", c_2 = "brain", and c_3 = "others", given MR images of the baby's brain. The aim is the visualization of brain development process of babies [15]. The classification of the skin and brain is necessary as an intermediate process. In MR images of the baby's brain, the skin and brain regions have relatively high contrasts compared with surrounding background regions. Although the skin regins have much higher MR values than the brain regions, the peripheral parts of the skin regins have often similar MR values to the brain regions due to partial volume effect. The image quality of volume rendering seriously degrade without the peripheral parts. The gradient magnitude can be used for the classification of the brain regions and the peripheral parts of the skin regins. While the peripheral parts of the skin regins have high gradient magnitude, the inside regions of the brain have low gradient magnitude. The two dimensional feature space is defined using the original MR value and the gradient magnitude, and can be effectively used for the classification.

3.2 Combining Simple Image Processing

The performance of the classifier can be further improved by combining simple image processing methods. These methods can be used to add the new feature axes in step 2 described in 3.1, and improve the quality of the classification as postprocessing of step 4.

3.2.1 Example 1: Combining selection of volume of interest

When the tissues of interest are sufficiently localized, and have sufficient contrast compared with neighboring tissues, the tissues of interests can be separated by specifying the volume of interest (VOI) whose shape is relatively simple and easy to specify, for example, ellipsoidal and rectangular. A new image is created, for example, by filling zero in the outside region of VOI and original values in the inside region. This new image can be regarded as defining the new axis of the multi-dimensional feature space, and naturally incorporated in step 2 described in 3.1.

3.2.2 Example 2: Combining morphological operation

The morphological operations such as erosion and dilation [16] can be applied to the classified results. These operations can smooth out the weight distribution of each tissue, and are used as postprocessing of step 4.

3.3 Selecting Opacity and Color

Tissue weight $w_i(\mathbf{x})$ determined by the method described in 3.1 is combined with the maximum tissue opacity α_i and tissue color $M_i = (r_i, g_i, b_i)$ in order to generate volume rendering images. The selection of the maximum tissue opacity α_i and tissue color $M_i = (r_i, g_i, b_i)$ is usually interactively performed by the user. This process is not trivial for the optimal visualization, and careful consideration is necessary for the selection.

3.4 Implementation

The implementation of the method described in this paper using a conventional volume rendering package is an interesting topic from the practical aspect. We implemented the method using VolPack [17], which is a portable software library based on a new family of fast volume rendering algorithms. VolPack generates color renderings from a three-dimensional image of scalar values. Our implementation is to select one axis to be interactively adjusted for each tissue, divide the full range assigned to scalar values of each voxel into segments with the number of tissues, and assign each segmented range to the axis of each tissue. However, rendering methods for classified multiple three-dimensional images [18] would be more suitable for the implementation.

Another important problem is interpolation to make each voxel isotropic. Although VolPack provides several interpolation routines including the Spline, we did not use them and used the sinc interpolation instead because some previous works reported that the results of maximum intensity projection (MIP) significantly improved even by just using sinc interpolation along the axial direction [19],[20]. The sinc function is performed by zero-filling expansion in a frequency domain. We applied the sinc interpolation to original 3D images before 3D filtering for the local structure computation.

4 Experimental Results

We applied the method to several different medical applications [1]. The method was implemented on Sun Enterprise server using multi-threaded programming.

4.1 Visualization of Bronchial Trees and Blood Vessels in Lung

Figure 1 shows the visualization results from chest CT images. In endoscopic biopsy via bronchial trees of lung, it is crucial on the accuracy of bioply to understand the structures of bronchial trees in advance, especially peripheral structures. Also, the relation to vessel structures is important. The vessel structures in the lung CT are easy to classify only using original CT images.

We used 30 slices (256 × 256 pixels) of CT images. The pixel size was 0.29 × 0.29 (mm) while the slice thickness was 1.0 (mm). After adjusting the window width and level of the CT values for bronchus visualization, we performed the sinc interpolation to make the voxels isotropic. Further, we applied the multi-scale line filter with $\sigma = \{1.5, 2.0, 3.0, 4.5\}$ (pixels). Figure 1 shows the volume rendering results based on the original image only, and the combination with the line-filtered image. Combining the line-filtered images significantly improved the visibility of thin bronchus structures.

4.2 Visualization of Brain Development Process of Baby

Figure 2 shows the visualization results of the brain development process of a baby from MR images. Pediatricians want to see the brain development process called myelination with relation to brain and skin surfaces [15]. The myelination is the process of creating myelin sheath. The range of MR values of the brain surfaces overlaps the range of myelin tissues.

We used 124 slices (256 × 256 pixels) of MRI images. The pixel size was 0.7 × 0.7 (mm) while the slice thickness was 1.5 (mm). After the sinc interpolation, the sheet

---

[1]All the volume rendering images shown in this paper are originally color images. The original color images show the advantages of the method much more clearly. Please contact the first author via email (yoshi@image.med.osaka-u.ac.jp) to see the original color images.

filter with $\sigma = 1.0$ (pixels) was used to enhance the brain surfaces. Also, the method described in 3.1.2 was combined. The tissue classification was performed using the three-dimensional feature space defined by the original, sheet-filtered, and gradient magnitude ($\sigma = 1.0$ pixels) images.

4.3 Visualization of Brain for Neurosurgical Planning and Navigation

Figure 3 shows the visualization results from brain MR images. The vein structures of brain surface are suggested to be useful as landmarks for surgical planning and navigation [14]. Thus, the aim was the visualization of the relations of the skin, the vessels, and the tumor. Because the tumor was located near the ventricle in this case, the ventricle was also needed to be visualized.

We used 80 slices (220×150 pixels) of MR (SPGR) image. The pixel size was 1.0×1.0 (mm) while the slice thickness was 1.2 (mm). After we performed the sinc interpolation to make the voxels isotropic, we applied the multi-scale line filter with $\sigma = \{0.8, 1.0, 1.2, 1.6, 2.0\}$ (pixels). The ventricle and the tumor had sufficient contrast compared with surrounding tissues and were easy to be trimmed using the method described in 3.2.1. These tissues were trimmed by specifying ellipsoids, respectively. The tissue classification was performed using the four-dimensional feature space defined by the original, line-filtered, and two trimmed images.

4.4 Visualization of Bone Tumor of Pelvis

Figure 4 shows the visualization results from pelvis CT images. Clinicians' concern was to localize bone tumors with relation to pelvis structures [21].

We used 50 slices (512×512 pixels) of MRI images. The pixel size was 1.0×1.0 (mm) while the slice thickness was 5 (mm). The cortices of bone, which are healthy parts of bone, and the bone tumor had similar CT values. After the sinc interpolation, the sheet filter with $\sigma = 1.0$ (pixels) was used to enhance the cortices of bone. The tissue classification was performed using the two-dimensional feature space defined by the original and sheet-filtered images.

5 Conclusion

We have described 3D image filters for the enhancement of specific local structures such as line and sheet. These filters have been shown to be effective for tissue classification of volume rendering. It should be emphasized that manual operations are minimized in our method. Thus, the method does not burden the users with heavy interactions. We believe that the use of 3D local intensity structures significantly enlarges the scope of volume rendering especially in the medical domain. We are now considering the comparison of our method and conventional volume rendering by the quantitative evaluation of image quality of rendering results.

References

[1] M.Levoy: Volume Rendering: Display of Surfaces from Volume Data, *IEEE Computer Graphics and Applications*, pp.29-36 (May 1988)

[2] R.A.Drebin, L.Carpenter, and P.Hanrahan: Volume Rendering, *Proc. SIGGRAPH*, pp.65-73 (August 1988).

[3] G.D.Rubin, C.F.Beullieu, V.Anngiro, *et al.*: Perspective Volume Rendering of CT and MR Images: Applications for Endoscopic Imaging, *Radiology*, Vol.199, pp.321-330 (1996).

[4] P.T. Johnson, D.G. Heath, B.S. Kuszyk, *et al.*: CT Angiography with Volume Rendering: Advantages and Applications in Splanchnic Vascular Imaging, *Radiology*, Vol.200, pp.564-568 (1996).

[5] Christian Barillot: Surface and Volume Rendering Techniques to Display 3-D Data: *IEEE Engineering in Medicine and Biology*, pp.111-119 (March 1993).

[6] M.Vannier, R.Butterfield, D.Jordon, and W.Murphy, *et al.*: Multi-Spectral Analysis of Magnetic Resonance Images, *Radiology*, Vol.154, pp.221-224 (1985).

[7] M.C.Clark, L.O.Hall, D.B.Goldgof, L.P.Clarke, R.P.Velthuizen, and M.S.Silbiger: MRI Segmentation using Fuzzy Clustering Techniques, *IEEE Engineering in Medicine and Biology*, pp.730-742 (November/December 1994).

[8] Y.Sato, S.Nakajima, H.Atsumi, *et al.*: 3D Multi-Scale Line Filter for Segmentation and Visualization of Curvilinear Structures in Medical Images, *Proc. First Joint Conference of CVRMed II and MRCAS III* (in press).

[9] H.Knutsson, Representing Local Structure Using Tensors, *Proc. the 6th Scandinavian Conference on Image Analysis*, pp.244-251 (June 1989).

[10] C-F Westin: A Tensor Framework for Multidimensional Signal Processing. Thesis No. 348, ISBN 91-7871-421-4, Linkping University, Sweden, (1994).

[11] T.M.Koller,G.Gerig,G.Szekely, *et al.*: Multiscale Detection of Curvilinear Structures in 2-D and 3-D Image Data, *Proc. ICCV*, pp.864-869 (1995).

[12] Y.Sato, J.Chen, N.Harada, *et al.*: Automatic Extraction and Measurement of Leukocyte Motion in Microvessels Using Spatiotemporal Image Analysis, *IEEE Trans. on Biomedical Engineering* (in press).

[13] R.Kikinis, P.L. Gleason, T.M. Moriarty, *et al.*: Computer-assisted Interactive Three-dimensional Planning for Neurosurgical Procedures, *Nerurosurgery*, Vol.38, pp.640-651 (1996).

[14] S.Nakajima, H.Atsumi, T.M.Moriarty, *et al.*: The Use of Cortical Surface Vessel Registration for Image-Guided Neurosurgery, *Nerurosurgery* (submitted).

[15] P.S.Huppi, M.Tsuji, T.Kapur, *et al.*: Quantification of changes in postnatal brain development in preterm infants using adaptive segmentation of MRI data, In Proceedings of Society of Magnetic Resonance and European Society for Magnetic Resonance in Medicine and Biology Joint Meeting, Nice, France, P.117, (August 1995).

[16] J.Serra: Image Analysis and Mathematical Morphology, London, Academic Press (1982).

[17] P.Lacroute and M.Levoy; Fast Volume Rendering Using a Shear-Warp Factorization of the Viewing Transform, *Proc. SIGGRAPH*, pp.451-458 (1994).

[18] A.Bhalerao, M.Halle and R.Kikinis: Volume Rendering Multiple Volumes using minimal 3D Depth Information (in preparation).

[19] N.M.Hylton, I.Simovsky, A.J.Li, *et al.*: Impact of Section Doubling on MR Angiography, *Radiology*, Vol.185, No.3, pp.899-902 (1992).

[20] Y.P.Du, D.L.Parker, W.L.Davis, *et al.*: Reduction of Partial-Volume Artifacts with Zero-filled Interpolation in Three-dimensional MR Angiography, *Journal of Magnetic Resonance Imaging*, Vol.4, No.5, pp.733-741 (1995).

[21] N.Shiraga, E.Kohda, K. Hiramatsu, Y.Sato, F.A. Jolesz, and R.Kikinis: 3-D Demonstration of the Osteosclerotic Lesion by Volume Rendering Method – New Possibility of Demonstrating Bone Tumor by Using 3-D Sheet Filter – (in preparation).
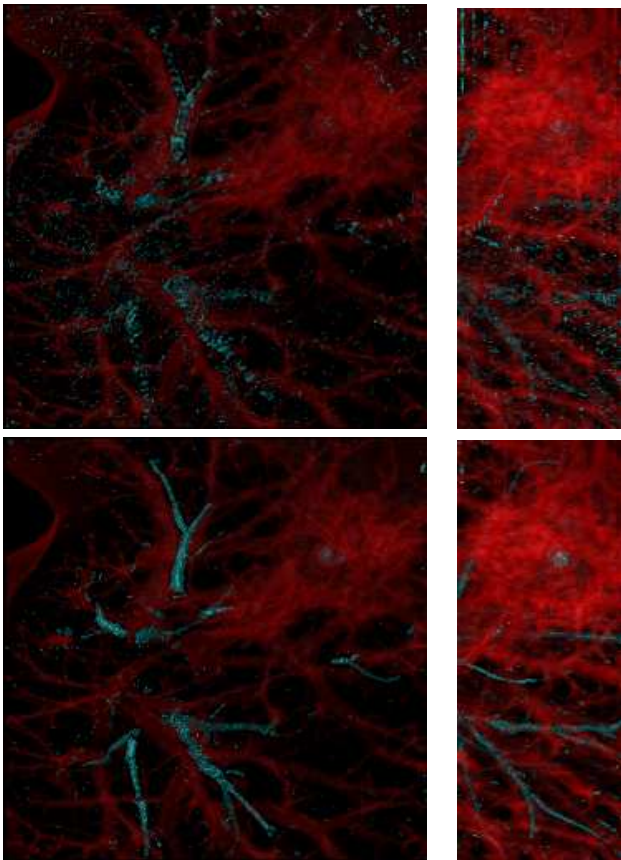
Figure 1: Bronchus and vessel visualization from lung CT. Top: Tissue classification based on original image. Bottom: Tissue classification based on original image and multi-scale line-filtered image.
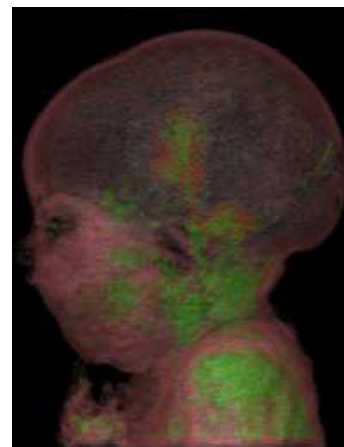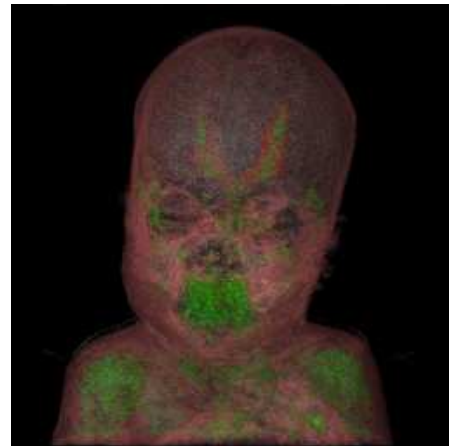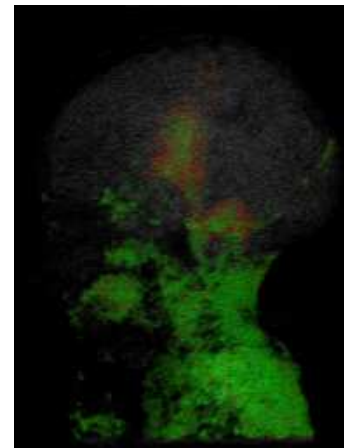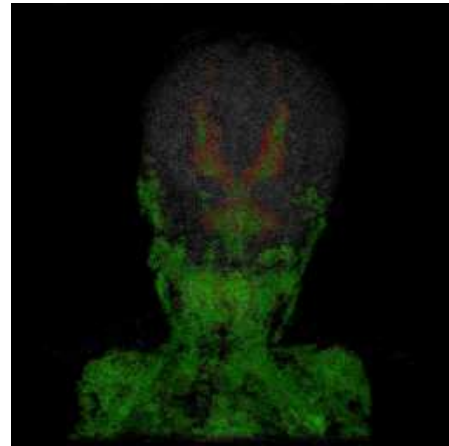

Figure 2: Visualization of brain development process of baby from MRI.
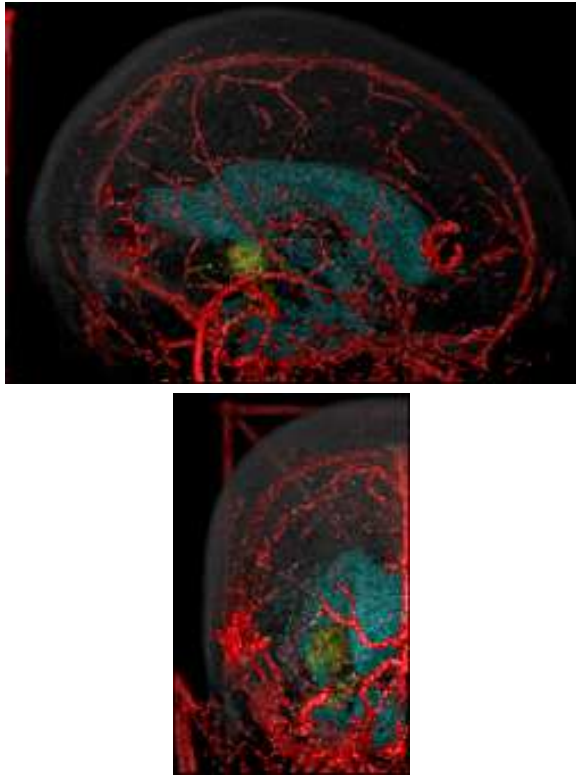
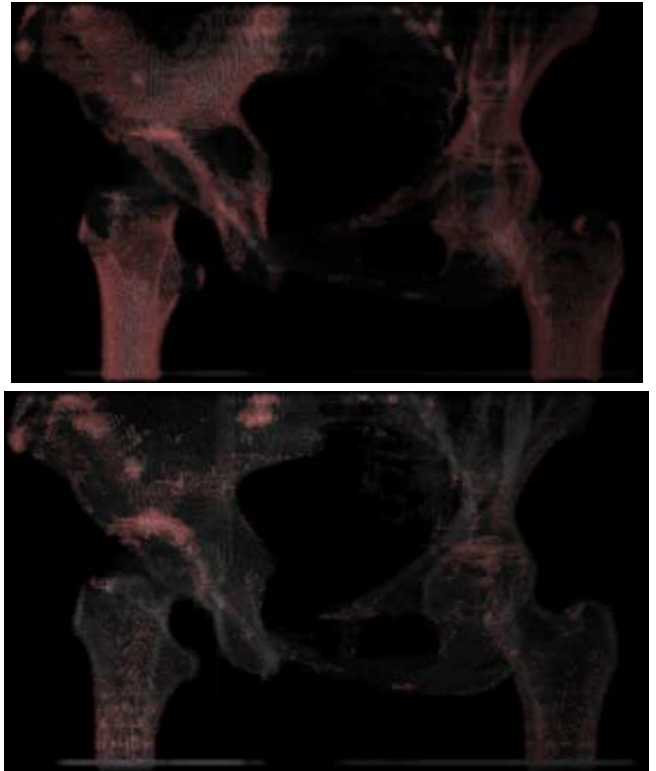Figure 3: Visualization of skin, vessels, ventricle, and tumor from brain MRI.

Figure 4: Visualization of bone tumor of pelvis from CT. Top: Tissue classification based on original image. Bottom: Tissue classification based on original and sheet-filtered images.